Synthesis of Multiband Frequency Selective Surfaces Using Machine Learning With the Decision Tree Algorithm

LEIDIANE C. M. M. FONTOURA [ID][1], **HERTZ WILTON DE CASTRO LINS** [ID][1],
ARTHUR S. BERTULEZA [ID][1], **ADAILDO GOMES D'ASSUNÇÃO** [ID][1], (Life Member, IEEE), AND
ALFRÊDO GOMES NETO [ID][2], (Senior Member, IEEE)

[1]Department of Communication Engineering, Federal University of Rio Grande do Norte (UFRN), Natal 59078-970, Brazil
[2]Federal Institute of Education, Science and Technology of Paraiba (IFPB), João Pessoa 58015-905, Brazil

Corresponding author: Adaildo Gomes D'Assunção (adaildo@ct.ufrn.br)

ABSTRACT This paper presents the synthesis of multiband frequency selective surfaces (FSSs) using supervised machine learning (ML) with the decision tree (DT) algorithm. The proposed FSS structure is composed of an array of metallic patches printed on a dielectric substrate for stopband spatial filtering microwave applications. The shapes of the metallic patches are based on the sunflower (*helianthus annus*) geometry. In the first step, a parametric analysis is performed to investigate the use of different FSS geometries, including those with circular, annular and corolla integrated patch elements, to compose the sunflower geometry, regarding multiband and polarization independent performances with size reduction. Two bioinspired FSS geometries are synthesized using supervised machine learning with the decision tree algorithm. The random forest (RF) algorithm is used to validate the decision tree algorithm and to confirm the obtained results. The numerical analysis of the proposed FSS geometries is performed using Ansoft Designer software. Prototypes are fabricated and measured. The good agreement observed between simulated and measured results has validated the proposed approach. The use of supervised machine learning with the decision tree algorithm resulted in a particularly efficient and accurate synthesis procedure due to its intuitive implementation and simplified and effective data analysis modelling.

INDEX TERMS Bioinspired FSS, decision tree, FSS, machine learning, multiband FSS, spatial filter.

I. INTRODUCTION

A typical frequency selective surface (FSS) is composed of a planar periodic array of metallic patches printed on a dielectric substrate presenting a stopband spatial filtering performance at microwaves frequencies [1]. Similarly, a FSS can be composed of a periodic array of apertures (or slots) perforated on a thin metallic sheet placed over a dielectric substrate exhibiting a passband filtering response at microwaves frequencies. Usually, the frequency behavior of the FSS depends on the geometry of the planar array elements, periodicity of the array, relative permittivity and thickness of the dielectric substrate, incident wave polarization, and incidence angle. Recently, the FSS geometries are being

used in many system applications, such as radar, satellite, wireless communication, and chipless RFID, at microwaves and millimeter waves [2], [3].

To meet the specific requirements of these communication systems, it is necessary to develop even more efficient and accurate FSS analysis and synthesis techniques. Many studies are available in the literature on the analysis, optimization and synthesis of FSSs [4]–[20].

The Equivalent Circuit Method (ECM) and artificial intelligence methods have been used in FSS analysis, optimization and synthesis, for example. Generally, ECM is used in the analysis and/or synthesis of structures with simple geometries. In [4], a novel dual-band reflected PCM (polarization converted metasurface) is proposed with a transmission window at 12.5 GHz and a −3 dB bandwidth of about 1.3 GHz (11.6 to 12.9 GHz). A coupled structure is used which is

composed of two FSSs with square rings, one grating, placed between them, and a PCM. Simulation and measurement results are in good agreement. In [5], a number of limbs and the different working modes of the single layer FSS unit cell is used to generate the two flexible adjustable transmission zeros, where the transmission pole is 4 GHz, and its bandwidth achieves 0.62 GHz. In [6], the values of periodicity and size of the array are obtained through calculations of the capacitive admittance and resistance of the FSS by a simple analytic method based on the transmission line theory. In [7], the analysis and the synthesis use the Genetic Algorithm (GA) with ECM, where the physical dimensions are obtained through the stop band, pass band and resonance frequency. More complex geometries generate new reactive elements that significantly increase the analytical complexity of the analysis, as in [8], where the ECM is used to determine the impedance matching network of transmission zeros and poles of the two-layer FSS and, as in [9], where the odd- and even-mode analysis is used to investigate the working mechanism of the FSS based on coupled stubs-loaded ring resonators.

Recently, in [10], authors used GRNN (General Regression Neural Network) with Multi-Objective Flower Pollination Algorithm (MOFPA) to obtain the physical dimensions from the desired resonance frequencies. In [11], authors used PSO (Particle Swarm Optimization) to determine the value of air gap in the bandwidth optimization of two coupled FSSs. In [12], the FSS synthesis is performed using a hybrid multi-objective bioinspired method, combining a GRNN network and an optimization algorithm (MOCS - Multi-Objective Cuckoo Search), where the dimensions and periodicity of geometry are obtained from resonance frequency and bandwidth estimations. In [13] and [14], the physical dimensions are obtained from the desired resonance frequencies using GA with ANN (Artificial Neural Network), and WCIP (Wave Concept Iterative Process), respectively. In [15], the dimensions of geometry are obtained from the angle of incident wave and resonance frequency desired. In [16] and [17], authors used fractal (Vicsek and Koch, respectively) in the analysis of single resonance frequency band FSS: in [16], authors used a bioinspired algorithm (SSO - Social Spider Optimization), and in [17] a simple numerical method to optimize the bandwidth of two coupled FSSs is reported. In [18] and [19], authors present FSS analysis with a third-level fractal characteristic, modified Jerusalem Cross (triple band) and Swastika (multiband), respectively. In [20], a single-layer FSS with an asymmetric Jerusalem cross patch, and a self-complementary aperture is proposed, based on the Babinet's principle.

This work presents a new proposal for the synthesis of multiband FSSs with conductive patch elements inspired on the sunflower geometry, with operating frequencies in the C and X bands. The main contributions are:

1) The use of machine learning with the decision tree algorithm in the synthesis of FSS spatial filters for communication systems;

2) The development of a fast, efficient and simplified solution, which reduces the complexity of the analysis of each sample, identifies the sensitivity of the project variables in the desired parameters, addresses conflicting objectives and has agility in training and synthesis;

3) The proposal of a new single layer FSS structure, which is symmetrical and exhibits angular stability and multiband frequency response, with printed sunflower-inspired conductive patch elements, which are compact, symmetrical and easy to fabricate;

4) The synthesis of a new FSS with triple band frequency behavior, with two closely spaced resonances, meeting the desired criteria of bandwidth, transmission coefficient and resonance frequency;

5) Validation of the accuracy of the methodology used, based on the agreement between simulation and measurement results.

Starting from the parameterization of the variables, the decision trees are trained and pruned, with analysis and validation of this algorithm by the random forest one. The generation of the dataset was obtained using Ansoft Designer software. Prototypes are fabricated and measured and a good agreement between simulation and measurement results is observed. Therefore, machine learning using the decision tree algorithm has proved to be a very attractive tool in the synthesis of FSS and, potentially, other planar integrated circuits for wireless communication systems.

This paper is organized as follows. The decision tree algorithm is briefly described in Section II. The design procedure of the FSS with sunflower-shaped patch elements is given in Section III. In Section IV, the numerical and experimental results are presented to validate the synthesis based on machine learning with the decision tree algorithm, and the conclusions are presented in Section V.

II. DECISION TREE ALGORITHM

Lately, the use of the machine learning technique has aroused the interest of researchers worldwide because it can learn from the data, identify patterns or classify outputs, and make decisions with minimal human intervention. The learning of the algorithm is performed automatically, as opposed to ANN, for example, in which the representative variables must be created manually. In addition, machine learning creates solutions from data or examples, and deals efficiently with conflicts of objectives. This is a different approach when compared to classical optimization methods, as for instance, GA, which search the space for possible solutions, and PSO, which investigates and creates new combinations in the search space. Among the applications, machine learning is used to control the propagation environment through intelligent walls [21], in wireless communication network applications [22], [23], and in optimizing data delivery rate in wireless sensor networks [24].

Decision trees (DT) are very intuitive Machine Learning tools. They are easy to interpret and easy to implement, and they can be defined as a union of concepts. They are

predictive and computational models, organized from the structure observed in trees, such as their branches and leaves. This branching structure can be applied to problems, such as classification [25]. In [26], DT is used to select the appropriate network, according to service characteristics and requirements (UMTS - Universal Mobile Telecommunication System, WLAN - Wireless Local Area Network, or WiMAX - Worldwide Interoperability for Microwave Access). In [27], DT is used to classify air quality using Wireless Sensor Network (WSN).

Similarly to the decision tree concept, random forests consist of a random selection of the predictor variables of the trees themselves. As presented, each individual tree is an enough simple model that has branches, nodes, and leaves. The random forest generates more independent trees, therefore reducing the correlation between the classifiers. Thus, the objective is to maintain the low bias of each individual classifier as it reduces variance. The random forest constitutes a conjunction of characteristics that culminates in the algorithm effective exercise, through inductions [28]. In this work, the branch reached by the trained model corresponds to classifications, from the characteristics defined in the mentioned classes, and their respective thresholds.

Fig. 1 presents an example of the classification process. The *Root Node* represents an entire population or sample and is further divided into two or more homogeneous sets. *Division* is the process of separating a node into two or more sub nodes. The *Decision Node* is obtained when a sub node is divided into additional sub nodes, and the *Terminal Node* or *Leaf* is the undivided node.

Then, the supervised decision tree and random forest methods were used to synthesize a FSS with three frequency bands. For the predictive modeling of the quantitative responses, the following steps of a machine learning system were used: random division of the data set into training and testing, preprocessing, learning, and prediction of the response of interest in test data and evaluation of data of the built models, as shown in Fig. 2.

A. DATA GENERATION AND SELECTION

Initially, the data generation is performed from parametric incursions, considering the project objectives in terms of resonance frequency, and other parameters. These incursions were guided by a correlation study of the behavior of the design variables and parameters considered.

In the data selection, the set was randomly divided into two subsets: training base and test base. Respectively, 70% of the observations were allocated for learning predictive models, and 30% for evaluation. Thus, the test base, represented by the remaining observations of the original data, is used to predict the models selected in the learning stage.

B. TREE TRAINING

For the synthesis process to be efficiently applied, it was necessary to insert three input parameters in the tree training process. Thus, the three resonance frequencies were defined
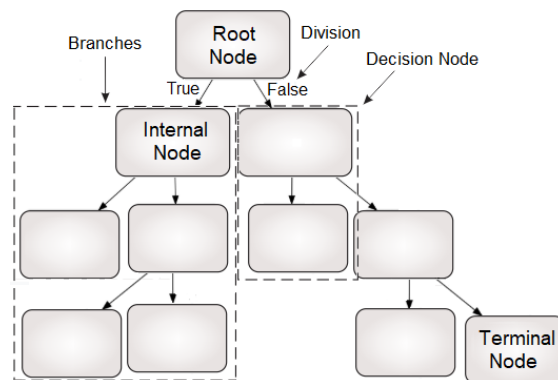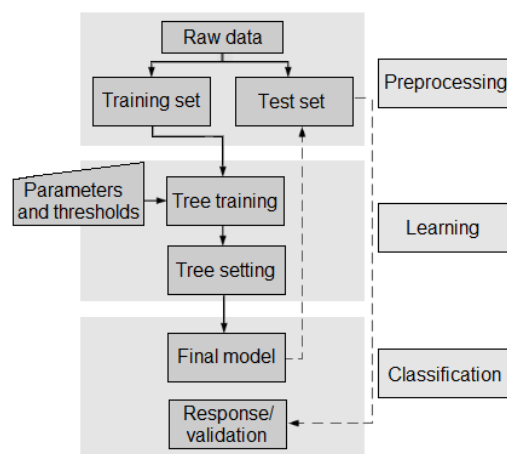

FIGURE 1. Decision tree representation.

FIGURE 2. Methodology used in the synthesis.

as parameters and thresholds, identified in Fig. 2. This leads to the generation of distinct trees whenever the parameters are changed. In addition, in order to avoid loss of accuracy or overlaps, resonance frequency limits were studied and determined, thus leading to trees with a high synthesis domain within the delimited values.

C. TREE SETTING (PRUNING)

In analyzing the criterion of the tree training process, it is noted that generating new nodes indefinitely can impair the prediction performance. Reaching leaves with a single sample will result in terminal nodes with only maximum purity. This can develop a confusing model with many rules and a significant chance of overfitting [29].

Otherwise, very shallow trees cannot reach all the information in the dataset. Thus, it is necessary to find a balance in the growth of decision trees so that the generalization error can be reduced.

The tree size is driven by some hyperparameters that can be calculated in order to better fit the model to the problem data. Knowing this, the algorithm hyperparameters (depth and criterion) were optimized with grid search and cross-validation [30].

III. FSS WITH SUNFLOWER-SHAPED PATCH ELEMENTS

In recent years, telecommunication systems requirements have imposed a continuous challenge to microwave engineers. Following natural evolution trained along billions of years, nature inspired geometries can provide interesting solutions, such as those reported for wireless system applications [31], [32]. In this work, the shape of the sunflower, scientifically called *helianthus annus* [33], is used as the FSS patch element shape in the parametric analysis. This geometry is symmetrical, enabling polarization independence, and is compact, enabling miniaturization and operation in three resonance bands. Moreover, it is easy to insert slotted rings. These characteristics are very suitable for FSS designs.

The triangular patch elements that represent the corolla (set of petals) increase the effective length of the ring loop, reducing its resonance frequency (in about 10%, considering the same design dimensions). In addition, the sunflower has the characteristic heliotropism, which contributes significantly to the increase in light interception. In other words, this movement allows the plant to act as a receiving antenna that automatically redirects it to receive the maximum solar radiation.

To obtain the sunflower geometry and its parameterization variables, the design procedure begins with a unit cell, with dimensions T_x, and T_y, and a circular patch with radius R, as shown in Fig. 3(a). A FSS with a circular patch and a slotted ring element, is indicated in Fig. 3(b), and a FSS with a circular patch and conducting petals, is illustrated in Fig. 3(c).
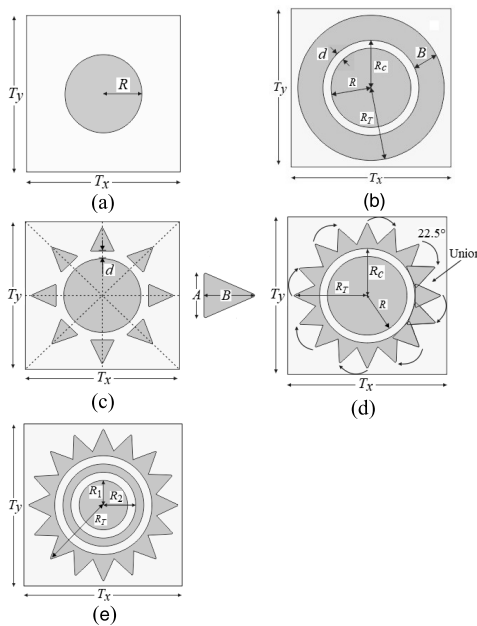

FIGURE 3. Evolution of the proposed sunflower inspired patch geometry. Patch element geometries are: (a) circular, (b) circular with slotted ring, (c) circular with petals, (d) sunflower with slotted ring and corolla (FSS1) and (e) sunflower with two slotted rings and corolla (FSS2).

The symmetry axis, diagonals, and dimensions A and B of the triangles representing the sunflower petals, that will form the corolla at the patch border, are shown in Fig. 3(c).

Each triangle has a thin metallization layer, with distance d from the circular patch. Thus, the triangles are doubled and rotated 22.5°, with the base points joined, creating a slot ring geometry with radius R_c, as shown in Fig. 3(d). Finally, a second slotted ring with inner radius R_1 and outer radius R_2 is inserted, composing the conducting patch geometry illustrated in Fig. 3(e). In the simulation of the corresponding FSS structure (FSS2), the unit cell is square, with $T_x = T_y$, and three dimensions are defined for parameterization: T_x, R_1 and R_2.

In this work, approximate expressions are used to obtain the initial dimensions of the unit cell geometry and estimate the resonance frequency in the design procedure. For a circular patch geometry with radius R, a good approximation for the resonance frequency, for $h \ll \lambda_0$, is given by (1), [34],

$$f_{res}\,(\text{GHz}) = \frac{0.3}{\pi R_{ef}\sqrt{\varepsilon_{ref}}} \quad (1)$$

where R_{ef} is the effective radius of the circular patch calculated using the approximate expression (2), as in [34], and ε_{ref} is the effective substrate dielectric constant given by (3).

$$R_{ef} = R\sqrt{1 + \frac{2h}{\pi R \varepsilon_{ref}}\left[ln\left(\frac{\pi R}{2h}\right) + 1.7726\right]} \quad (2)$$

$$\varepsilon_{ref} = \frac{\varepsilon_r + 1}{2} \quad (3)$$

where R is the radius of the conducting patch and ε_r is the substrate relative permittivity. The calculation of the resonance frequency corresponding to the slotted ring with radius R_c, as shown in Fig. 3(b), is performed using (4), (2) and (3). For the frequency corresponding to the ring representing the corolla, the effective radius of $R_c + B$, represented by R_T, as illustrate in Figs. 3(d) and 3(e), is calculated using (4), (2) and (3), replacing R_{cef} with the value of R_{Tef}.

$$f_{res}\,(\text{GHz}) = \frac{0.3}{4R_{cef}\sqrt{\varepsilon_{ref}}} \quad (4)$$

IV. NUMERICAL AND EXPERIMENTAL RESULTS

A. FSS1 RESULTS

A FSS structure with the patch element geometry illustrated in Fig. 3(d), defined as FSS1, was designed and simulated. Numerical characterization was performed using Ansoft Designer, a computer program based on the Method of Moments (MoM) [35]. A prototype was fabricated on a FR-4 substrate with relative permittivity $\varepsilon_r = 4.4$, thickness $h = 1.57$ mm, and loss tangent $tan\delta = 0.02$, for comparison purpose. In the frequency range used, the dispersion of the relative permittivity of the FR-4 substrate is very small and was neglected. The unit cell dimensions are $T_x = T_y = 20$ mm and the FSS1 structure is composed of 10×10 elements, with overall dimensions of 200 mm × 200 mm, as shown in Fig. 4(a). The patch dimensions are $R = 5$ mm and $R_c = 6$ mm, $A = 3$ mm, $B = 3.2$ mm and $d = 1$ mm.

To identify the estimated frequency, ε_{ref}, R_{ef}, R_{cef}, R_{Tef} values are 2.7, 5.59 mm, 6.63 mm, and 9.91 mm, respectively.
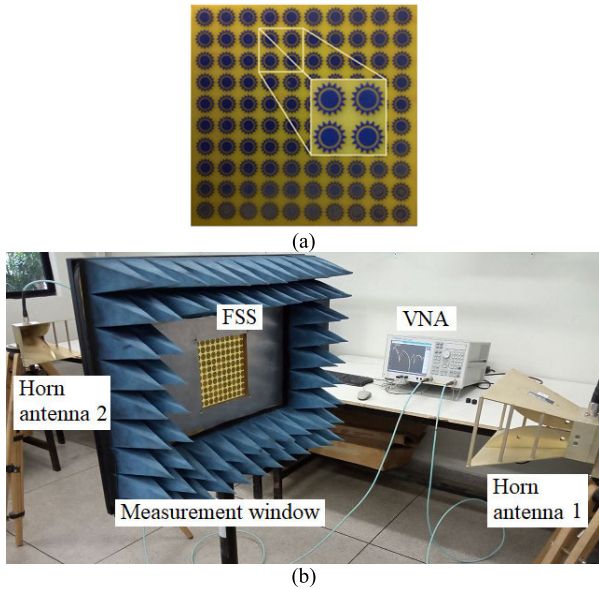
(a)

(b)

FIGURE 4. Photos of: (a) FSS1 prototype and (b) Measurement setup.
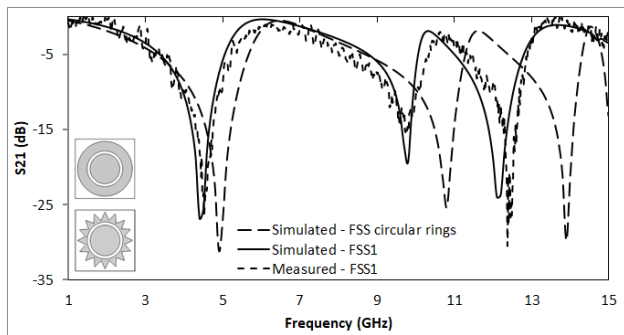

FIGURE 5. Transmission coefficient results for two FSSs, one with circular patch and slotted ring element, Fig. 3(b), and the other one with circular patch, slotted ring and corolla elements (FSS1), Fig. 3(d). $Tx = Ty = 20$ mm, $R = 5$ mm, $R_c = 6$ mm, $A = 3$ mm, $B = 3.2$ mm, and $d = 1$ mm.

Experimental results were obtained using an Agilent N5071C vector network analyzer (VNA) along with a pair of double ridge waveguide horn antennas, SAS-571. The measurement setup is shown in Fig. 4(b), with the identification of the instruments and equipment used and the indication of the FSS location with respect to the transmitting and receiving antennas. The wave incidence is considered normal to the surface of the FSS1.

Fig. 5 presents frequency response results of the FSS1 structure and of the FSS with circular and slotted ring patch, for TE-polarization, but due to symmetry similar results are obtained for TM polarization. The triangular ring conductive element type (corolla) causes the first resonance, as expected. The ring slot type, which emerges through the union of triangles, enables resonance frequency in 6.88 GHz, with result determined using (4) with (2) and (3). The surface current density distribution for both cases is illustrated in Fig. 6(a), at 4.4 GHz, and Fig. 6(b), at 6.1 GHz, where the maximum value is shown in red color and the minimum
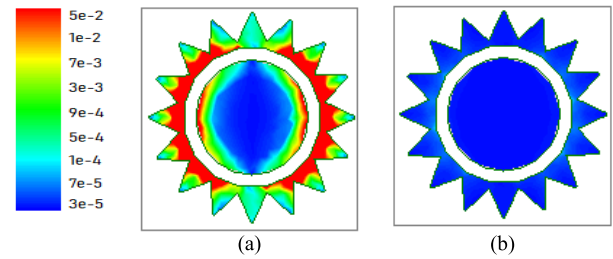

(a)   (b)

FIGURE 6. Electric current density ($J_{max} = 0.05$ A/m^2) on the FSS1 structure conducting patch element, Fig. 3(d), at (a) 4.4 GHz (with resonance) and (b) 6.1 GHz (without resonance).

TABLE 1. Frequency results of FSS1 and FSS with circular patch with a slotted ring element.

Result (GHz)	FSS1			FSS with circular rings		
	F_1	F_2	F_3	F_1	F_2	F_3
Estimated	4.60	10.39	-	4.60	10.39	-
MoM	4.40	9.80	12.20	4.90	10.80	13.90
Measured	4.64	9.89	12.41	-	-	-

value in blue color. As expected, FSS1 resonates at 4.4 GHz, but not at 6.1 GHz.

In Fig. 5 it is interesting to observe the FSS1 triple band operation, ranging from 3.92 GHz to 4.75 GHz, 9.44 GHz to 9.96 GHz, and 11.62 GHz to 12.50 GHz. For the FSS with circular patch and slotted ring elements the resonance bands are from 4.20 GHz to 5.34 GHz, 10.10 GHz to 11.10 GHz, and 13.30 GHz to 14.17 GHz. Fig. 6 confirms that FSS1 reduces the resonance frequency values by increasing the effective length of the circular ring of the conductive element. The results of the resonance frequencies of these structures are presented in Table 1.

B. DATA AND ALGORITHMS DISCUSSION
Table 2 summarizes the parameterization variables results related to the chosen geometry, Fig. 3(e), defined as FSS2, and the upper and lower limits, considering the minimum spacing of 0.25 mm between R_1 and R_2. In the high-resolution dataset (10 MHz frequency step), 462 samples were generated without repetition. Thus, after training the decision tree, the synthesis was performed using the Phyton 3.7 language as a tool [36]. The patch dimensions are $R = 5$ mm, $R_c = 6$ mm, $A = 3$ mm and $B = 3.2$ mm.

Two different scenarios were considered based on the criteria informed to the algorithm. S_1: F_1, F_2, and F_3 with values of 4.2 GHz, 9.5 GHz, and 10.5 GHz, respectively, and S_2: frequencies 4.2 GHz, 9.0 GHz, and 10.5 GHz, respectively. Initially, markings are performed to identify the training classes. Thus, three classes were created: *Insufficient*, *Average*, and *Ideal*, included in Table 3, where F_0 is the desired frequency. From this, it is possible to measure bandwidth, transmission coefficient and resonance frequency. The data were collected

TABLE 2. Limits and steps of parameterization variables.

Variable (mm)	Lower Limit	Upper Limit	Step
T_x	19.00	22.00	0.50
R_1	2.00	4.50	0.25
R_2	2.25	4.75	0.25

TABLE 3. Problem parameters classification.

Parameter	Insufficient	Average	Ideal
F_R (GHz)	$F_R \geq 10\% \, F_0$	$5\% \, F_0 \leq F_R < 10\% \, F_0$	$F_R < 5\% \, F_0$
BW (GHz)	$BW \leq 0.07$	$0.07 < BW \leq 0.12$	$BW > 0.12$
$\|S21\|$ (dB)	$\|S21\| \geq -12$	$-20 \leq \|S21\| < -12$	$\|S21\| < -20$

TABLE 4. Decision tree training and evaluation results.

Parameter	Accuracy (%)	F1 score (%)	Max Depth	Criterion	Cross-Validation
BW_1	99.281	99.281	3	Gini	10
BW_2	99.281	99.281	3	Gini	10
BW_3	93.525	93.525	7	Gini	10
$S21_1$	99.281	99.281	3	Gini	10
$S21_2$	98.561	98.561	7	Entropy	10
$S21_3$	94.245	94.245	7	Entropy	10
F_{R1}	99.281	99.281	6	Entropy	10
F_{R2}	98.561	98.561	6	Gini	10
F_{R3}	96.403	96.403	7	Entropy	10

TABLE 5. Random forest training and evaluation results.

Parameter	Accuracy (%)	F1 score (%)	Max Depth	Criterion	N estimators
BW_1	99.281	99.281	3	Gini	100
BW_2	99.281	99.281	3	Gini	100
BW_3	90.647	90.647	7	Entropy	100
$S21_1$	99.281	99.281	3	Gini	100
$S21_2$	97.842	97.842	3	Gini	100
$S21_3$	90.647	90.647	7	Entropy	100
F_{R1}	97.842	97.842	3	Gini	100
F_{R2}	94.964	94.964	3	Gini	100
F_{R3}	92.806	92.806	7	Entropy	100
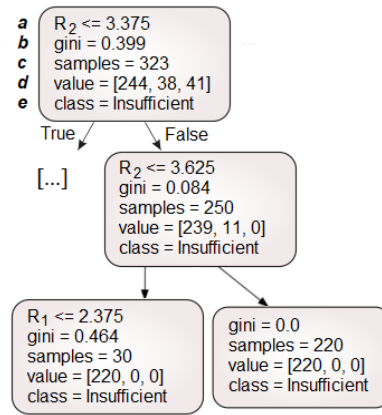
FIGURE 7. Identified branch of the decision tree used in the synthesis.

based on what is desired: the frequency values that have application in wireless communication systems, the bandwidth required for information transmission, and the acceptable level of S21. During the process, the tree was pruned to undesirable values, improving accuracy significantly. In this way, all the decision making is performed by the algorithm.

Using the decision tree first, several tuples (results) are obtained satisfying the problem. Thus, observing that the most relevant parameters are R_1 and R_2, two tuples were selected for experimental characterization. In both cases, the periodicity is the same because it has little influence on the behavior of the frequency response. Thus, under criteria with *Ideal* classification, their respective $[T_x, R_1, R_2]$ values for each scenario are (in mm) [19, 2.25, 2.75] and [19, 2, 3].

In the implementation, there are 9 distinct decision tree algorithms and 9 random forest algorithms, trained by the dataset with 70% of 462 samples obtained by numerical characterization of the following parameters: BW_1, $S21_1$, F_{R1}, at first, BW_2, $S21_2$, F_{R2}, at second, and BW_3, $S21_3$, F_{R3}, at third resonance bands. Table 3 shows the limits of the classification parameters used in each algorithm. In both scenarios, under the same criteria, the random forest returned the same tuples: [19, 2.25, 2.75], [19, 2.5, 2.75], [19, 2, 3].

Tables IV and V present the results of the learning (training) and evaluation (testing) stages of the predictive models. The metric used to measure and optimize models during learning was accuracy. The performance evaluation of the models showed satisfactory execution, with accuracy higher than 0.90 for all classifiers. The best results were observed for the decision tree model. The root node, with the highest information gain, defines R_2 as the largest factor in determining the rating (slot ring radius).

As shown in Fig. 7, in the branch identified in the tree, there is in the root node, a subdivision of parameters, where (a), (b), (c), (d), and (e) are: index with the highest information gain (from that point); impurity measure; number of observations from the classification of this node; number of samples that are in each class (0 for *Insufficient*, 1 for *Average*, and 2 for *Ideal*); and most characteristic classification on the sheet. Thus, following this part of the tree, the nodes on the left are *True* and the nodes on the right are *False*. There are 250 observations to classify: 220 are classified as insufficient and 30 remain in another decision node to finalize the classification. From this point, the biggest information gain is R_1 (patch radius).

C. FSS2 RESULTS

A synthesis procedure based on machine learning with the decision tree algorithm was applied to the geometry of the proposed frequency selective surface (FSS2), which consists of the periodic array of patch elements presented in Fig. 3.2(e).
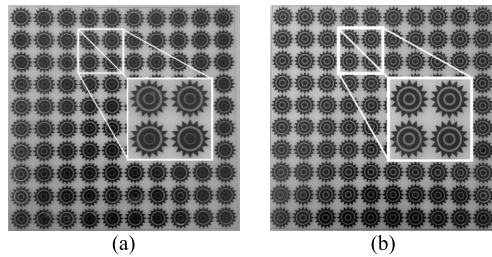
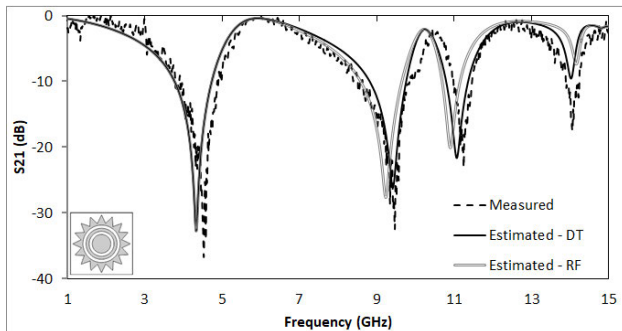FIGURE 8. Photos of FSS2 prototypes for scenarios: (a) S_1 and (b) S_2.

FIGURE 9. Frequency response results of the transmission coefficient of FSS2. synthesized according scenario S_1, with triple bands at 4.2 GHz, 9.5 GHz, and 10.5 GHz. Structural parameters: $Tx = Ty = 19$, $R = 5$, $R_c = 6$, $A = 3$, $B = 3.2$, $d = 1$, $R_1 = 2.25$ and $R_2 = 2.75$. All dimensions in mm.
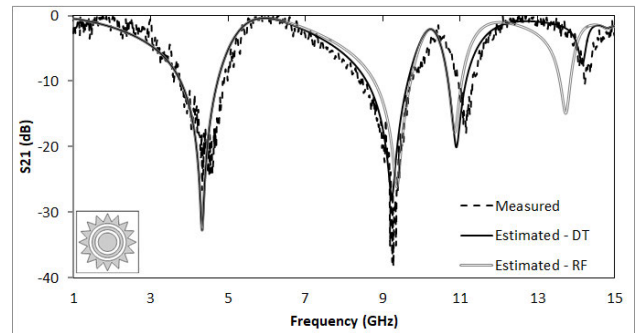

FIGURE 10. Frequency response results of the transmission coefficient of FSS2. synthesized according scenario S_2, with triple bands at 4.2 GHz, 9.0 GHz, and 10.5 GHz. Structural parameters: $Tx = Ty = 19$, $R = 5$, $R_c = 6$, $A = 3$, $B = 3.2$, $d = 1$, $R_1 = 2$ and $R_2 = 3$. All dimensions in mm.

TABLE 6. Comparison between FSS2 results for scenario S_1.

Parameter	Measured	DT	RF
BW_1 (GHz)	1.09	0.97	0.98
BW_2 (GHz)	1.33	0.96	1.08
BW_3 (GHz)	0.46	0.58	0.47
$S21_1$ (dB)	-36.73	-32.74	-32.76
$S21_2$ (dB)	-32.26	-26.11	-27.65
$S21_3$ (dB)	-23.07	-21.65	-20.09
F_{R1} (GHz)	4.52	4.33	4.33
F_{R2} (GHz)	9.47	9.42	9.23
F_{R3} (GHz)	11.24	11.07	10.9

TABLE 7. Comparison between FSS2 results for scenario S_2.

Parameter	Measured	DT	RF
BW_1 (GHz)	1.16	0.98	0.97
BW_2 (GHz)	1.33	1.08	0.96
BW_3 (GHz)	0.36	0.47	0.36
$S21_1$ (dB)	-26.59	-32.76	-32.73
$S21_2$ (dB)	-38.21	-27.65	-26.12
$S21_3$ (dB)	-17.93	-20.09	-17.82
F_{R1} (GHz)	4.33	4.33	4.33
F_{R2} (GHz)	9.27	9.23	9.37
F_{R3} (GHz)	11.15	10.90	10.86

The FSS2 square unit cell dimensions Tx, R_1 and R_2, shown in Fig. 3.2(e), were parameterized. The remaining FSS2 patch element dimensions are: R = 5 mm, R_c = 6 mm, A = 3 mm, B= 3.2 mm and d = 1 mm, and dielectric substrate parameters are: ε_r = 4.4, h = 1.57 mm, and $\tan\delta$ = 0.02, as used in FSS1.

The synthesis of FSS2 is performed for two different scenarios, aiming to obtain resonance frequencies at a) F_1 = 4.2 GHz, F_2 = 9.5 GHz and F_3 = 10.5 GHz (scenario S_1), and b) F_1 = 4.2 GHz, F_2 = 9.0 GHz and F_3 = 10.5 GHz (scenario S_2).

The calculated results for the FSS2 geometry, for scenario S1, are Tx = 19 mm, R_1 = 2.25 mm and R_2 = 2.75 mm. These results were used to fabricated the FSS2 prototype shown in Fig. 8(a). For scenario S_2, the calculated values are T_x = 19 mm, R_1 = 2 mm and R_2 = 3 mm, which were used to fabricate the prototype shown in Fig. 8(b). In both scenarios, the FSS2 overall dimensions are 190 mm × 190 mm. After training the decision tree, the synthesis obtained by the desired criteria occurs within 10 s computation time. The hardware setup of the used computer system is AMD Ryzen 5 3500U processor with 8 GB installed memory.

TE-polarization and normal incidence were assumed. Nevertheless, due to the symmetry of the FSS2 patch elements, similar results for the transmission coefficient S21 are expected for TM polarization.

To validate the results obtained by the decision tree, two tuples obtained by the random forest were chosen: [19, 2, 3] and [19, 2.5, 2.75] for scenarios S_1 and S_2, respectively.

The choice method was based on the relevance and the lowest mean value of the errors of each parameter.

Figs. 9 and 10 show the frequency response of the FSS2 configurations for scenarios S_1 and S_2, respectively. As expected, the tuples meet the imposed conditions and the synthesis, performed at the three resonance frequencies of the structure, has a significant portion of values in the *Ideal* classification. In addition, it is important to note that the fourth resonance frequency (14.09 GHz) of FSS2 becomes more pronounced in the measured result, with S21 level and bandwidth equal to −15.74 dB and 0.33 GHz, respectively. Tables VI and VII show the comparison between the results obtained by the DT and RF methods and those characterized

TABLE 8. Comparison between qualitative and quantitative parameters of FSS synthesis reported in literature.

Ref.	Analysis/ Synthesis	Structure	Geometry	Element size (mm)	Frequency band/ Operation range	Resonance frequency (GHz)	Method
[6]	Yes/Yes	isolated	Square patch	9	X/ Single	10	ECM
[7]	Yes/Yes	isolated	Square loop and quasi-open square loop	4.2	X/ Single	8.76; 8.44	ECM + GA
[8]	Yes/No	coupled (2)	Jerusalem ring and hexagonal patch with ring	6*	Ku/ Single	16.1	ECM
[9]	Yes/No	coupled (3)	Stubs-loaded ring	10*	C/ Single	6.02	ECM
[10]	Yes/Yes	isolated	Lozenge-shaped	13.5	X/ Single	15.2	GRNN + MOFPA
[11]	Yes/No	coupled (2)	Crossed dipole	9.87	X/ Single	9.87	PSO
[12]	Yes/Yes	isolated	Triangular ring	6.4	X/ Single	11	GRNN + MOCS
[13]	Yes/Yes	isolated	Crossed dipole	12	X/ Single	8.15; 9.19	GA + ANN
[14]	Yes/Yes	isolated	Parallel metallic strips	20*	C/ Dual; X/ Triple	7, 9.4 (x), and 9.1, 11.2 (y); 6.1, 9.3, 10.5 (x), and 6.1, 8.3, 10.7 (y)	WCIP
[15]	Yes/Yes	isolated	Square loop	7.34	C/ Single	5.389	ANN + GEANN
[16]	Yes/No	isolated	Vicsek Fractal	8.30	X/ Single	9.17	SSO
[17]	Yes/No	coupled (2)	Koch Fractal	10*	X/ Single	8.33, 9.15	Numeric Method
[18]	Yes/No	isolated	Modified Jerusalem Cross (Fractal)	20.5	L, C, X/ Multiband	1.78; 6.42; 8.69; 10.94; 12.98	CST
[19]	Yes/No	isolated	Swastika Fractal	14	C, X/ Triple	4.2; 10.1; 13.3	FEM (HFSS)
[20]	Yes/No	isolated	Asymmetric Jerusalem Cross	4*	X, Ku/ Multiband	11.963; 17.565; 15.845	CST
This work	Yes/Yes	isolated	Bioinspired (combined element)	18.4	C, X/ Triple	4.2, 9.5, 10.5; 4.2, 9.0, 10.5	DT

*Size of unit cell in x

experimentally. It can be concluded that the presented results are in good agreement.

For the resonance frequencies, the errors between the predicted values from the ML approach and the expected values, are lower than 5% (Table 3). In addition, all the criteria concerning the minimum bandwidth of 0.12 GHz and the maximum transmission coefficient of −20 dB (Table 3) were fulfilled simultaneously, at three resonance bands.

Table 8 presents a comparison between the parameters obtained in this work and those of works available in the literature.

V. CONCLUSION

An application of machine learning with the decision tree algorithm was used in the synthesis of two stopband FSS structures, the first one with operating frequencies at (a) 4.2 GHz, 9.5 GHz, and 10.5 GHz, and the second one at 4.2 GHz, 9.0 GHz, and 10.5 GHz.

A single layer FSS structure printed on a FR-4 substrate, with an array of sunflower inspired patch elements, was used to provide stopband response with miniaturization and polarization independence. Simulation was performed using Ansoft Designer software.

Accurate numerical results were obtained meeting the required criteria of a minimum bandwidth of 0.12 GHz and a maximum transmission coefficient of -20 dB, at the three resonance bands, simultaneously.

About the machine learning with the decision tree performance, it should be highlighted its agility in algorithm training, efficiency and speed in synthesis, accurate response based on the desirable criteria presented, and this is an intuitive method easy to interpret and easy to implement.

Prototypes were fabricated and tested for validation of the proposed approach. A good agreement was observed between simulation and measurements results, as well as predictive classification methods. Therefore, the proposed method has been proven to be unquestionably attractive for the synthesis of FSS structures.

REFERENCES

[1] B. A. Munk, "General overview," in *Frequency Selective Surfaces—Theory and Design*. New York, NY, USA: Wiley, 2000, pp. 14–21.

[2] S. Shrestha, M. Balachandran, M. Agarwal, V. V. Phoha, and K. Varahramyan, "A chipless RFID sensor system for cyber centric monitoring applications," *IEEE Trans. Microw. Theory Techn.*, vol. 57, no. 5, pp. 1303–1309, May 2009, doi: 10.1109/TMTT.2009.2017298.

[3] A. L. P. de Siqueira Campos, R. H. C. Maniçoba, and A. G. d'Assunção, "Investigation of enhancement band using double screen frequency selective surfaces with koch fractal geometry at millimeter wave range," *J. Infr., Millim., THz Waves*, vol. 31, no. 12, pp. 1503–1511, Dec. 2010, doi: 10.1007/s10762-010-9735-8.

[4] M. Yan, J. Wang, Y. Pang, C. Xu, H. Chen, L. Zheng, J. Zhang, and S. Qu, "An FSS-backed dual-band reflective polarization conversion metasurface," *IEEE Access*, vol. 7, pp. 104435–104442, Jul. 2019, doi: 10.1109/ACCESS.2019.2931551.

[5] Y. Ma, Y. Yuan, D. Wang, Q. Shi, and N. Yuan, "A way to design the miniaturized dual-stopbands FSS based on the topology structure," *IEEE Access*, vol. 7, pp. 156536–156543, 2019, doi: 10.1109/ACCESS.2019.2947310.

[6] A. Firouzfar, M. Afsahi, and A. A. Orouji, "Novel synthesis formulas to design square patch frequency selective surface absorber based on equivalent circuit model," *Int. J. RF Microw. Comput.-Aided Eng.*, vol. 29, pp. 1–9, Feb. 2019.

[7] A. L. P. S. Campos, A. M. Martins, and V. A. Almeida Filho, "Synthesis of frequency selective surfaces using genetic algorithm combined with the equivalent circuit method," *Microw. Opt. Technol. Lett.*, vol. 54, no. 8, pp. 1893–1897, Aug. 2012.

[8] Y. Ma, W. Wu, Y. Yuan, W. Yuan, and N. Yuan, "A high-selective frequency selective surface with hybrid unit cells," *IEEE Access*, vol. 6, pp. 75259–75267, 2018, doi: 10.1109/ACCESS.2018.2878941.

[9] R.-X. Liao, S.-W. Wong, Y. Li, J.-Y. Lin, B.-Y. Liu, F.-C. Chen, and Z. Quan, "Quasi-elliptic bandpass frequency selective surface based on coupled stubs-loaded ring resonators," *IEEE Access*, vol. 8, pp. 113675–113682, 2020, doi: 10.1109/ACCESS.2020.3003319.

[10] M. C. D. A. Neto, H. R. O. Ferreira, J. P. L. de Araújo, F. J. B. Barros, A. G. Neto, M. O. Alencar, and G. P. dos Santos Cavalcante, "Compact ultra-wideband FSS optimised through fast and accurate hybrid bio-inspired multiobjective technique," *IET Microw., Antennas Propag.*, vol. 14, no. 9, pp. 884–890, Jul. 2020, doi: 10.1049/iet-map.2019.0821.

[11] H. W. C. Lins, E. L. F. Barreto, and A. G. d'Assunção, "Enhanced wideband performance of coupled frequency selective surfaces using metaheuristics," *Microw. Opt. Technol. Lett.*, vol. 55, no. 4, pp. 711–715, Apr. 2013, doi: 10.1002/mop.27451.

[12] M. C. A. Neto, J. P. L. Araújo, F. J. B. Barros, A. N. Silva, G. P. S. Cavalcante, and A. G. D'Assunção, "Bioinspired multiobjective synthesis of X-band FSS via general regression neural network and cuckoo search algorithm," *Microw. Opt. Technol. Lett.*, vol. 57, no. 10, pp. 2400–2405, Oct. 2015, doi: 10.1002/mop.29349.

[13] R. M. S. Cruz, P. H. da F. Silva, and A. G. D'Assuncao, "Synthesis of crossed dipole frequency selective surfaces using genetic algorithms and artificial neural networks," in *Proc. Int. Joint Conf. Neural Netw.*, Jun. 2009, pp. 627–633, doi: 10.1109/IJCNN.2009.5178927.

[14] K. Bencherif, M. Titaouine, R. Saidi, A. Djouimaa, I. Adoui, T. R. D. Sousa, A. G. Neto, and H. Baudrand, "Multiband FSS analysis and synthesis based on parallel non coupled metallic strips using WCIP method," *J. Microw., Optoelectron. Electromagn. Appl.*, vol. 17, no. 4, pp. 433–456, Oct. 2018.

[15] S. Moinzad and A. Abdolali, "A new efficient approach for fast and accurate design of frequency selective surfaces based on geometry estimation networks," *Neural Comput. Appl.*, vol. 28, no. 9, pp. 2727–2734, Sep. 2017.

[16] P. S. Oliveira, A. G. D'Assunção, E. A. M. Souza, and C. Peixeiro, "A fast and accurate technique for FSS and antenna designs based on the social spider optimization algorithm," *Microw. Opt. Technol. Lett.*, vol. 58, no. 8, pp. 1912–1917, Aug. 2016, doi: 10.1002/mop.29941.

[17] R. H. C. Maniçoba, A. F. Santos, A. V. Lovato, N. M. Oliveira-Neto, D. B. Brito, A. L. P. S. Campos, and A. G. d'Assunção, "Numerical investigation of multilayer fractal FSS," *Int. J. Mod. Eng. Res. Technol.*, vol. 4, no. 5, pp. 24–30, May 2014.

[18] H. V. H. S. Filho, C. P. N. Silva, M. R. T. D. Oliveira, E. M. F. D. Oliveira, M. T. D. Melo, T. R. D. Sousa, and A. G. Neto, "Multiband FSS with fractal characteristic based on Jerusalem cross geometry," *J. Microw., Optoelectron. Electromagn. Appl.*, vol. 16, no. 4, pp. 932–941, Dec. 2017.

[19] M. Fallah, A. H. Nazeri, and M. R. Azadkhah, "A novel fractal multi-band frequency selective surface," *J. Microw., Optoelectron. Electromagn. Appl.*, vol. 18, no. 2, pp. 276–285, Jun. 2019, doi: 10.1590/2179-10742019v18i21559.

[20] H. Wang, H. Yan, S. Qu, L. Zheng, and J. Wang, "Design of a self-complementary frequency selective surface with multi-band polarization separation characteristic," *IEEE Access*, vol. 7, pp. 36788–36799, 2019, doi: 10.1109/ACCESS.2019.2905416.

[21] L. Subrt and P. Pechac, "Controlling propagation environments using intelligent walls," in *Proc. 6th Eur. Conf. Antennas Propag. (EUCAP)*, Mar. 2012, pp. 1–5, doi: 10.1109/EuCAP.2012.6206517.

[22] C. Jiang, H. Zhang, Y. Ren, Z. Han, K.-C. Chen, and L. Hanzo, "Machine learning paradigms for next-generation wireless networks," *IEEE Wireless Commun.*, vol. 24, no. 2, pp. 98–105, Apr. 2017, doi: 10.1109/MWC.2016.1500356WC.

[23] M. Chen, U. Challita, W. Saad, C. Yin, and M. Debbah, "Artificial neural networks-based machine learning for wireless networks: A tutorial," 2017, *arXiv:1710.02913*. [Online]. Available: http://arxiv.org/abs/1710.02913

[24] Y. Wang, M. Martonosi, and L.-S. Peh, "A supervised learning approach for routing optimizations in wireless sensor networks," in *Proc. 2nd Int. Workshop Multi-Hop ad Hoc Netw., From Theory Reality (REALMAN)*, May 2006, pp. 79–86, doi: 10.1145/1132983.1132997.

[25] S. S.-Shwartz and S. B.-David, "Decision trees," in *Understanding Machine Learning: From Theory to Algorithms*. New York, NY, USA: Cambridge Univ. Press, 2014, pp. 250–256.

[26] W.-H. Li and Z. Qi, "Network selection algorithm based on decision tree in heterogeneous wireless networks," in *Proc. MATEC Web Conf.*, vol. 189, Jan. 2018, pp. 1–7, doi: 10.1051/matecconf/201818904010.

[27] B. Sugiarto and R. Sustika, "Data classification for air quality on wireless sensor network monitoring system using decision tree algorithm," in *Proc. 2nd Int. Conf. Sci. Technol.-Comput. (ICST)*, Oct. 2016, pp. 172–176, doi: 10.1109/ICSTC.2016.7877369.

[28] N. Farnaaz and M. A. Jabbar, "Random forest modeling for network intrusion detection system," *Procedia Comput. Sci.*, vol. 89, pp. 213–217, Jan. 2016, doi: 10.1016/j.procs.2016.06.047.

[29] F. Esposito, D. Malerba, G. Semeraro, and J. Kay, "A comparative analysis of methods for pruning decision trees," *IEEE Trans. Pattern Anal. Mach. Intell.*, vol. 19, no. 5, pp. 476–491, May 1997, doi: 10.1109/34.589207.

[30] *Tuning the Hyper-Parameters of an Estimator*. Accessed: Jan. 2021. [Online]. Available: https://scikit-learn.org/stable/modules/grid_search.html

[31] L. C. M. de Moura, J. D. N. Cruz, A. P. da Costa, P. H. D. F. Silva, and J. C. e Silva, "UWB cotton leaf design microstrip-fed printed monopole antenna," in *IEEE MTT-S Int. Microw. Symp. Dig.*, Nov. 2015, pp. 1–4, doi: 10.1109/IMOC.2015.7369155.

[32] A. P. Singh, "A leaf shaped microstrip patch antenna," *Int. J. Sci., Eng. Technol. Res.*, vol. 2, no. 4, pp. 807–809, Apr. 2013.

[33] D. S. Rivero, O. M. Mahecha, A. J. Gonzalez, M. S. Rivero, A. E. Puentes, and J. O. Aguilar, "Composition and behavior of sunflower seeds (Helianthus Annuus L.) from plants treated with magnetic fields for energy potential use of biomass," *Chem. Eng. Trans.*, vol. 65, pp. 679–684, Jun. 2018.

[34] C. A. Balanis, "Microstrip antennas," in *Antenna Theory: Analysis and Design*, 3rd ed. Hoboken, NJ, USA: Wiley, 2005, pp. 811–826.

[35] *Ansoft Designer*. Accessed: Jan. 2021. [Online]. Available: http://www.ansys.com

[36] *Python Software*. Accessed: Jan. 2021. [Online]. Available: https://www.python.org/

LEIDIANE C. M. M. FONTOURA received the B.Sc. degree in telecommunications from the Federal Institute of Education, Science and Technology of Goiás, Brazil, in 2012, and the M.Sc. degree in advanced electromagnetism from the Federal Institute of Education, Science and Technology of Paraíba, João Pessoa, Brazil, in 2015. She is currently pursuing the Ph.D. degree in electrical engineering and computation with the Federal University of Rio Grande do Norte (UFRN), Natal, Brazil.

She is a member of the Microwave and Antenna Group–GMA, UFRN. Her research interests and activities include periodic structures, frequency selective surfaces, antennas, and machine learning.
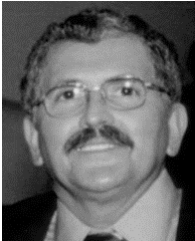
HERTZ WILTON DE CASTRO LINS received the M.S. and Ph.D. degrees in electrical engineering and computation from the Federal University of Rio Grande do Norte, Brazil, in 2006 and 2012, respectively.

He has been with the Federal University of Rio Grande do Norte, since 2012, where he is currently a Full Professor. He is teaching and conducting research on frequency selective surfaces, antennas, propagation, wireless, electromagnetism and sensors communications, artificial intelligence, machine learning, and bio inspired algorithms. He is a member of the Brazilian National Institute on Wireless Communications (INCT-CSF) and a Researcher at the Innovation and Health Laboratory (LAIS), Federal University of Rio Grande do Norte. He has coauthored ten journal articles, two book chapters, and five conference papers.
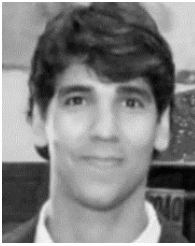
ARTHUR S. BERTULEZA received the Bachelor of Science and Technology degree (Hons.) from the Federal University of Rio Grande do Norte (UFRN), Brazil, in 2019, where he is currently pursuing the Bachelor of Telecommunications Engineering degree.

His research interests include antennas, electromagnetism, wireless, neural networks, artificial intelligence, and machine learning.

ADAILDO GOMES D'ASSUNÇÃO (Life Member, IEEE) received the B.S.E.E. degree (Hons.) from the Federal University of Rio Grande do Norte (UFRN), Brazil, in 1974, and the M.S. and Ph.D. degrees in electrical engineering from the State University of Campinas, Brazil, in 1977 and 1981, respectively.

From 1975 to 1976, he worked in radar and telemetry systems at the Launching Center of Barreira do Inferno, Natal, Brazil. He has been with the Federal University of Rio Grande do Norte, since 1976, where he is currently a Full Professor of electrical and electronics engineering. From 1985 to 1987, he was a Postdoctoral Visiting Scientist at North Dakota State University, USA. He is a Coordinator of the Brazilian National Institute on Wireless Communications (INCT-CSF). He is teaching and conducting research on frequency selective surfaces, antennas, propagation, wireless communications, millimeter waves, and terahertz. He has coauthored 98 journal articles, three book chapters, and 189 conference papers. His interests include reconfigurable, flexible and wearable integrated circuits, EBG devices, ceramic substrates, and metamaterials.

Dr. D'Assunção is a member of the Brazilian Microwave and Optoelectronics Society (SBMO). He chaired the 1997 and 2011 SBMO/IEEE MTT-S International Microwave and Optoelectronics Conference (IMOC). He was a Former President of SBMO, from 2000 to 2002. He received the UFRN/FUNPEC Research Prize, in 2004. He received the SBMO Professor Attílio José Giarola Medal of Merit, in 2012.

ALFRÊDO GOMES NETO (Senior Member, IEEE) received the B.Sc., M.Sc., and D.Sc. degrees in electrical engineering and microwaves area from the Federal University of Paraíba, Campina Grande, Brazil, 1986, 1989, and 1994, respectively.

In 1993, he developed part of his D.Sc. at the ENSEEIHT, INPT, Toulouse, France, to where he returned, in 2005, during the postdoctorate researches. Since 1989, he has been with the Federal Institute of Paraíba, IFPB. In 1994, he was a Founder of the Group of Telecommunications and Applied Electromagnetism, GTEMA, IFPB. He has more than 170 papers published in journals and conferences. His research interests include electromagnetic theory, microwaves, wave propagation, FSS, antennas, and numerical methods.

Dr. Gomes Neto is a member of the Brazilian Society of Microwaves and Optoelectronics, SBMO, and Institute of Electrical and Electronics Engineers, Inc. (IEEE). He was the General Chair of the Brazilian Microwave Symposium, in 2000.

• • •